PERGAMON International Journal of Multiphase Flow 24 (1998) 1139–1161

International Journal of Multiphase Flow

Viscous liquid film flows over a periodic surface

Yu. Ya. Trifonov *

Institute of Thermophysics, Siberian Branch of Russian Academy of Sciences, Novosibirsk, 630090, Russia

Received 28 February 1997; received in revised form 15 April 1998

Abstract

The paper is devoted to a theoretical analysis of a viscous liquid film flowing down a vertical one-dimensional periodic surface. The investigation is based on both Navier–Stokes and integral equations and performed over a wide range of Reynolds number and surface geometry characteristics taking into account viscosity, inertia and surface tension. Shape of the film free surface and streamline function are calculated. It is shown that there are two ranges of parameters where the film flow is controlled by surface tension or inertia forces and where qualitatively different behavior of the flow main characteristics is obtained. Stagnation zones are found and their transformation with increasing Reynolds number is investigated. Comparison with experimental data is carried out.

Keywords: Viscous liquid film flow; Periodic surface

1. Introduction

Theoretical studies of film flows began with the classical work of Nusselt (1916) where he obtained exact solutions for Navier–Stokes equations for a thin layer of viscous liquid free falling down a smooth vertical wall:

$$U_0(y) = \frac{3\nu Re}{H_0}\left[\frac{y}{H_0} - \frac{y^2}{2H_0^2}\right], \quad H_0 = \left[\frac{3\nu^2 Re}{g}\right]^{1/3}.$$

Here $U_0(y)$ is a velocity profile in the film in the direction of gravity vector g; ν is the kinematic viscosity; H_0 is the liquid layer thickness at a given flow rate; Re is the Reynolds number.

* Corresponding author.

0301-9322/98/$19.00
PII: S0301-9322(98)00022-6

Further theoretical and experimental investigations have demonstrated that the Nusselt solution is not achieved in practice and, as a rule, the film surface is covered with waves. A great number of works have been devoted to both linear and non-linear analysis of wave formation and there are many reviews devoted to wavy films (Fulford, 1964; Alekseenko et al., 1992).

The problem of non-linear waves in the film falling down a smooth surface has much in common with that of a viscous layer flow along a corrugated surface. In both cases the governing equations are significantly non-linear, the free surface is previously unknown, the surface tension forces play a great role and there exists a spatial period. In our investigations we will use some ideas of the numerical method developed by Trifonov and Tsvelodub (1991) in their investigation of nonlinear steady-state traveling waves. At the present time, there are a few theoretical papers and only one experimental work devoted to film flows along corrugated surfaces. Using perturbation theory, Wang (1981) investigated the flow along a sinusoidal surface with a corrugation amplitude that was small compared to the Nusselt's thickness. Kang and Chen (1995) generalized this approach on two-layers flowing down an inclined, slightly wavy surface. Using boundary-integral computational analysis, Pozrikidis (1988) considered a creeping flow over an inclined periodic surface when the inertia forces were ignored. Shetty and Cerro (1993) developed asymptotic analysis of flow when the film thickness is much smaller than the amplitude of corrugation and it was demonstrated that the influence of the inertia and surface tension forces is small in this case. Zhao and Cerro (1992) obtained experimental data on flow over different types of corrugated surface.

2. Governing equations

We consider a flow of viscous incompressible liquid along a vertical corrugated surface. A schematic of the flow and the coordinate system are shown in Fig. 1. The equations of motion

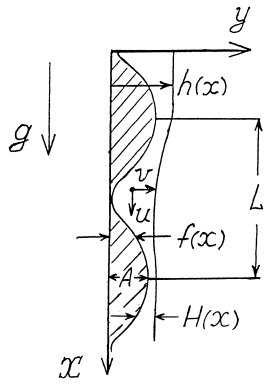

Fig. 1. Flow scheme.

and boundary conditions are as follows:

$$u\frac{\partial u}{\partial x}+v\frac{\partial u}{\partial y}=-\frac{1}{\rho}\frac{\partial P}{\partial x}+g+v\left[\frac{\partial^2 u}{\partial x^2}+\frac{\partial^2 u}{\partial y^2}\right];$$

$$u\frac{\partial v}{\partial x}+v\frac{\partial v}{\partial y}=-\frac{1}{\rho}\frac{\partial P}{\partial y}+v\left[\frac{\partial^2 v}{\partial x^2}+\frac{\partial^2 v}{\partial y^2}\right];\quad \frac{\partial u}{\partial x}+\frac{\partial v}{\partial y}=0$$

$$u=v=0,\quad y=f(x);$$

$$\sigma_{ik}n_k n_i=-P^{(\mathrm{V})}+\frac{\sigma}{\left[1+\left(\frac{\mathrm{d}h}{\mathrm{d}x}\right)^2\right]^{3/2}}\frac{\mathrm{d}^2 h}{\mathrm{d}x^2},\quad \sigma_{ik}n_k\tau_i=0,\quad i,k=1,2,\quad y=h(x);$$

$$v=u\frac{\mathrm{d}h}{\mathrm{d}x},\quad y=h(x).$$

Here, u is the velocity in the x-direction, v is the velocity in the y-direction, P is the pressure in the liquid; $P^{(\mathrm{V})}$ is the atmospheric pressure; ν and μ are the kinematic and dynamic viscosities, correspondingly; ρ is the liquid density; σ is the surface tension coefficient; $f(x)$ is the wall surface shape, $h(x)$ is the film free surface shape, $H(x)=h(x)-f(x)$ is the local film thickness, σ_{ik} is the stress tension components, n_k and τ_i are the components of normal and tangential unit vectors, respectively.

Summing over repeated indexes is assumed in the boundary conditions and to complete the definition of the equations we use the well-known formulas:

$$\mathbf{n}=\frac{\left(-\frac{\mathrm{d}h}{\mathrm{d}x},1\right)}{\sqrt{1+\left(\frac{\mathrm{d}h}{\mathrm{d}x}\right)^2}},\quad \boldsymbol{\tau}=\frac{\left(1,\frac{\mathrm{d}h}{\mathrm{d}x}\right)}{\sqrt{1+\left(\frac{\mathrm{d}h}{\mathrm{d}x}\right)^2}},\quad \mathbf{u}=(u,v),$$

$$\mathbf{x}=(x,y),\ \sigma_{ik}=-P\delta_{ik}+\mu\left(\frac{\partial u_i}{\partial x_k}+\frac{\partial u_k}{\partial x_i}\right).$$

After some transformation, the boundary conditions on the free surface can be presented as follows:

$$P=P^{(\mathrm{V})}+2\mu\frac{\partial v}{\partial y}\frac{1+\left(\frac{\mathrm{d}h}{\mathrm{d}x}\right)^2}{1-\left(\frac{\mathrm{d}h}{\mathrm{d}x}\right)^2}-\frac{\sigma}{\left[1+\left(\frac{\mathrm{d}h}{\mathrm{d}x}\right)^2\right]^{3/2}}\frac{\mathrm{d}^2 h}{\mathrm{d}x^2},\quad y=h(x);$$

$$\frac{\partial u}{\partial y}+\frac{\partial v}{\partial x}+4\frac{\partial v}{\partial y}\frac{\mathrm{d}h}{\mathrm{d}x}\frac{1}{1-\left(\frac{\mathrm{d}h}{\mathrm{d}x}\right)^2}=0,\quad y=h(x);$$

From the continuity equation and kinematic condition on the free surface we have the integral of motion

$$\int_{f(x)}^{h(x)} u(x, y)\,\mathrm{d}y = \text{const} = Q_0 = vRe. \tag{1}$$

Here, Q_0 is a flow rate in the liquid and Re is the Reynolds number.

The shape of the free surface is unknown beforehand. We use coordinates transformation: $x = x$, $\eta = [y - f(x)]/H(x)$ and the flow area becomes known: $x = [0, L]$, $\eta = [0, 1]$. Using the new variables $x^* = x/L$, $y^* = y/H_0$, $f^*(x) = f(x)/A$, $u^* = u/u_0$, $v^* = v/(\varepsilon u_0)$, $H^*(x) = H(x)/H_0$, $P^* = P/\rho u_0^2$, the non-dimensional equations are written as follows:

$$-\frac{\partial P}{\partial x} - \eta_x \frac{\partial P}{\partial \eta} + \frac{1}{\varepsilon Re}\left[3 + \eta_y^2 \frac{\partial^2 u}{\partial \eta^2} + \varepsilon^2\left[\frac{\partial^2 u}{\partial x^2} + \eta_x^2 \frac{\partial^2 u}{\partial \eta^2} + 2\eta_x \frac{\partial^2 u}{\partial x \partial \eta} + (\eta_{x\xi} + \eta_x \eta_{x\eta}) \frac{\partial u}{\partial \eta}\right]\right] - \eta_y \frac{\partial uv}{\partial \eta} - \frac{\partial u^2}{\partial x} - \eta_x \frac{\partial u^2}{\partial \eta} = 0; \tag{2}$$

$$\frac{\partial (P - P^{(\mathrm{V})})}{\partial \eta} = \frac{\varepsilon}{Re}\left[\eta_y^2 \frac{\partial^2 v}{\partial \eta^2} + \varepsilon^2\left[\frac{\partial^2 v}{\partial x^2} + \eta_x^2 \frac{\partial^2 v}{\partial \eta^2} + 2\eta_x \frac{\partial^2 v}{\partial x \partial \eta} + (\eta_{x\xi} + \eta_x \eta_{x\eta}) \frac{\partial v}{\partial \eta}\right]\right] \cdot H(x) - \varepsilon^2\left[H \frac{\partial uv}{\partial x} + H\eta_x \frac{\partial uv}{\partial \eta} + \frac{\partial v^2}{\partial \eta}\right]; \tag{3}$$

$$v(x, \eta) = -H(x) \cdot u(x, \eta) \cdot \eta_x - \frac{\partial}{\partial x}\left[H \int_0^{\eta} u(x, \eta')\,\mathrm{d}\eta'\right]; \tag{4}$$

$$H(x) \int_0^1 u(x, \eta')\,\mathrm{d}\eta' = 1; \tag{5}$$

$$u(x, \eta) = 0, \text{ for } \eta = 0; \tag{6}$$

$$P - P^{(\mathrm{V})} = \frac{2\varepsilon}{Re} \frac{1}{H(x)} \frac{\partial v}{\partial \eta} \frac{1 + \varepsilon^2\left[\dfrac{\mathrm{d}^2 H}{\mathrm{d}x^2} + \dfrac{1}{\varepsilon_1} \dfrac{\mathrm{d}^2 f}{\mathrm{d}x^2}\right]^2}{1 - \varepsilon^2\left[\dfrac{\mathrm{d}^2 H}{\mathrm{d}x^2} + \dfrac{1}{\varepsilon_1} \dfrac{\mathrm{d}^2 f}{\mathrm{d}x^2}\right]^2} - \varepsilon^2 We \frac{\dfrac{\mathrm{d}^2 H}{\mathrm{d}x^2} + \dfrac{1}{\varepsilon_1} \dfrac{\mathrm{d}^2 f}{\mathrm{d}x^2}}{\left[1 + \varepsilon^2\left[\dfrac{\mathrm{d}H}{\mathrm{d}x} + \dfrac{1}{\varepsilon_1} \dfrac{\mathrm{d}f}{\mathrm{d}x}\right]^2\right]^{3/2}}, \quad \text{for } \eta = 1; \tag{7}$$

$$\left[\frac{\partial u}{\partial \eta} + \varepsilon^2 H \frac{\partial v}{\partial x} - \varepsilon^2\left[\frac{\mathrm{d}H}{\mathrm{d}x} + \frac{1}{\varepsilon_1} \frac{\mathrm{d}f}{\mathrm{d}x}\right] \frac{\partial v}{\partial \eta}\right]\left[1 - \varepsilon^2\left[\frac{\mathrm{d}H}{\mathrm{d}x} + \frac{1}{\varepsilon_1} \frac{\mathrm{d}f}{\mathrm{d}x}\right]^2\right] + 4\varepsilon^2 \frac{\partial v}{\partial \eta}\left[\frac{\mathrm{d}H}{\mathrm{d}x} + \frac{1}{\varepsilon_1} \frac{\mathrm{d}f}{\mathrm{d}x}\right] = 0, \text{ for } \eta = 1. \tag{8}$$

Here A is the corrugation amplitude, $u_0 = Q_0/H_0$, $\varepsilon = H_0/L$, $\varepsilon_1 = H_0/A$, H_0 is the Nusselt film thickness, $We = (3Fi)^{1/3}/Re^{5/3}$, $Fi = (\sigma/\rho)^3/g\nu^4$, $\eta = (y - f(x)/\varepsilon_1)/H(x)$, $\eta_x = -(\eta \mathrm{d}H/\mathrm{d}x + (1/\varepsilon_1)\mathrm{d}f/\mathrm{d}x)/H(x)$, $\eta_y = 1/H(x)$, $\eta_{x\eta} = -(1/H)\ \mathrm{d}H/\mathrm{d}x$, $\eta_{x\xi} = -(\eta_x/H)\ \mathrm{d}H/\mathrm{d}x - (\eta \mathrm{d}^2H/\mathrm{d}x^2 + (1/\varepsilon_1)\mathrm{d}^2f/\mathrm{d}x^2)/H(x)$.

There are four independent parameters in the problem (e.g. Fi, $(\nu^2/g)^{1/3}/L$, A/L and Re) and a function describing the wall configuration $f(x)$. The problem consists of finding fields $u(x, y)$, $v(x, y)$, $P(x, y)$ and $H(x)$ at the given parameters. Eq. (2)–(5) were computed numerically with the use of the spectral method:

$$u(x,\eta) = \frac{1}{2}U_1(x) + \sum_{m=2}^{M} U_m(x)T_{m-1}(\eta_1), \quad \eta_1 = 2\eta - 1;$$

$$U_m(x) = U_m^0 + \sum_{\substack{n=-N/2+1 \\ n\neq 0}}^{N/2-1} U_m^n \exp[2\pi \mathrm{i} n x],\ (U_m^{-n})^* = U_m^n,\ m = 1, \ldots, M.$$

Here $T_m(\eta_1)$ are Chebyshev polynomials, and the 'star' superscript designates complex conjugation.

At $M(N-1)$ known values of harmonics U_m^n, the film thickness $H(x)$ is unambiguously regenerated from (5), $v(x, \eta)$ from (4), and $P(x, \eta)$ from (3) and (7). The numerical algorithm starts with the specification of the initial approximation for harmonics U_m^n which are then improved by Newton's method from (2) transformed into (n, m)-space. The Jacobian matrix was calculated using the first order differential scheme, and nonlinear terms in the equations were calculated in (x, η)-space.

Let us mention that when applying the spectral method, a common problem arises: with an account for boundary conditions (6), (8), we have $(M + 2)(N-1)$ nonlinear algebraic equations for the definition of $M(N-1)$ unknown values, i.e. the system is overdefined. This problem is related to the fact that the basic functions in spectral expansion do not satisfy boundary conditions. There are several ways to overcome this. In the current paper we discard $2(N-1)$ equations corresponding to the last two Chebyshev coefficients in the expansion of the right side of (2). While adjusting the procedure we tried other methods of reducing the number of equations and the results do not differ significantly for a good enough accuracy of approximation of the function $u(x, \eta)$ ($|U_m^{N/2-1}|/\sup|U_m^n| < 10^{-3}$ at any m, and $|U_M^n|/\sup|U_m^n| < 10^{-3}$ at any n). During the calculations, the indicated conditions of approximation were provided by the corresponding increase of numbers N and M from 16 to 128 and from 5 to 15, respectively, depending on the Reynolds number, surface geometry and physical properties of the liquid.

3. Integral model main equations

A number of recent publications have demonstrated (see Trifonov and Tsvelodub, 1991 and review by Alekseenko et al., 1992) that the integral approach describes well the wavy film hydrodynamics in the case of a flow down a smooth wall. The integral approach requires far fewer computer resources than do calculations based on the Navier–Stokes equations.

In the case of the wavy hydrodynamics, only the long-wave disturbances were considered by use of the integral approach. Let us restrict ourselves in the case of flowing over a corrugated surface to studying the films which are thin compared to the corrugation period [$\varepsilon \ll 1$, see (2)–(8)]. For the range of Reynolds numbers under consideration $\varepsilon \ll Re < 1/\varepsilon$, after neglecting terms smaller than $O(\varepsilon)$ the equations simplified substantially. In dimensional form it is as follows:

$$u\frac{\partial u}{\partial x} + v\frac{\partial u}{\partial y} = -\frac{1}{\rho}\frac{\partial P}{\partial x} + g + v\frac{\partial^2 u}{\partial y^2}; \quad \frac{\partial P}{\partial y} = 0; \tag{9}$$

$$\frac{\partial u}{\partial x} + \frac{\partial v}{\partial y} = 0; \quad u = v = 0, \quad y = f(x);$$

$$P = P^{(V)} - \sigma\frac{\mathrm{d}^2 h}{\mathrm{d}x^2}, \quad v = u\frac{\mathrm{d}h}{\mathrm{d}x}, \quad \frac{\partial u}{\partial y} = 0, \quad y = h(x).$$

Deriving (9) from (2)–(8) we retain the term containing the capillary pressure in the boundary condition. This is possible if the film number $Fi \backsim Re^5/\varepsilon^6$, which is generally true for most experiments.

For further simplification of the problem we will use the self-similarity assumption of the velocity profile:

$$u(x, y) = \frac{3vRe}{H(x)}\left(\frac{y - f(x)}{H(x)} - \frac{[y - f(x)]^2}{2H^2}\right). \tag{10}$$

The velocity profile given by (10) is the simplest expression that satisfies the boundary condition on the wall and free surface. For the flat plate Eq. (10) is the exact solution of the Navier–Stokes equation. We think that, for the case of long corrugations $\varepsilon \ll 1$, this assumption is reasonable enough. The correctness of (10) will be evaluated by comparing the solutions of the simplified system with the experimental results and with the solutions of Navier–Stokes equations.

Using (10) and integrating (9) over the y-direction from $f(x)$ to $h(x)$, we obtain a single differential equation as follows:

$$\frac{6}{5}\frac{\mathrm{d}}{\mathrm{d}x}\frac{1}{H} = \frac{3}{\varepsilon Re}\left(H - \frac{1}{H^2}\right) + \varepsilon^2 WeH\left[\frac{\mathrm{d}^3 H}{\mathrm{d}x^3} + \frac{1}{\varepsilon_1}\frac{\mathrm{d}^3 f}{\mathrm{d}x^3}\right]. \tag{11}$$

Here the units of the dimensionless values are the same as those of (2)–(8).

There are three independent parameters (εRe, $\varepsilon^2 We$, ε_1) in (11) that differ from (2)–(8) where we have four parameters. Eq. (11) was computed numerically by use of the Fourier expansion:

$$H(x) = \sum_{n=-N/2+1}^{N/2-1} H_n \exp[2\pi\imath nx], \quad (H_{-n})^* = H_n.$$

After substitution in (11), we have a system of nonlinear algebraic equations which were calculated numerically by Newton's method. Nonlinear terms were calculated in x-space and their Fourier-harmonics were determined later.

During the calculations the number of harmonics N was changed from 16 to 256 in order to provide accuracy of approximation $|H_{N/2}|/\sup|H_n| < 10^{-3}$.

4. Results of the numerical calculations and comparison with experiments

Some results of calculations on the basis of Navier–Stokes Eqs. (2)–(8) and the integral model (11) are presented in Figs. 2 and 3, respectively. Fig. 4 demonstrates the experimental data obtained by Zhao and Cerro (1992). For all the figures, the film flow of highly viscous liquids (silicon oil and glycerol) was investigated and shapes of the free surface (lines 1 S–19 S) are shown with the Reynolds number decreasing (see Table 1 for the values of Re). Amplitude and period of corrugation are equal to $A = f_{\max}(x) - f_{\min}(x) = 3.175$ mm, $L = 6.35$ mm, respectively, for both calculation and experiment. The dimensionless form of the solid surface

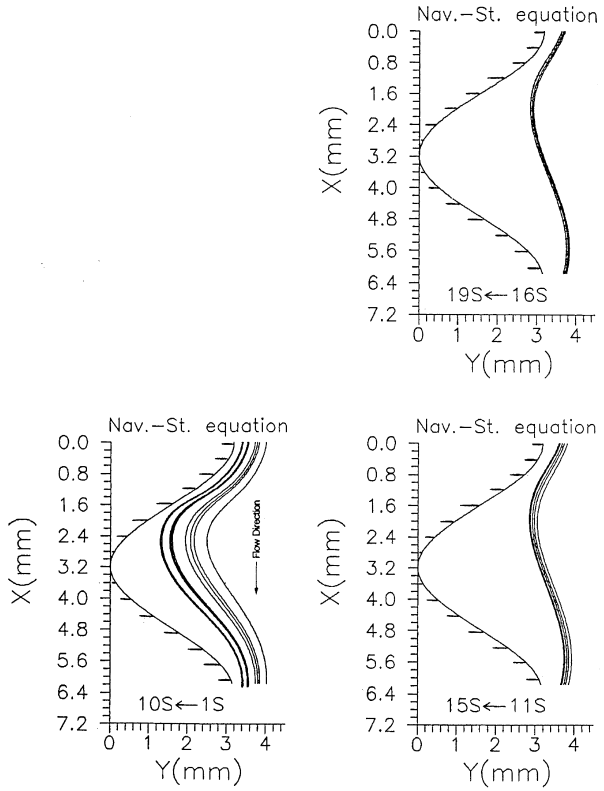

Fig. 2. Free surface profiles of the silicon oil film flowing over the corrugated surface with $A = 3.175$ mm and $L = 6.35$ mm. Calculations based on the Navier–Stokes equations and flow rates corresponding to lines 1 S–19 S are given in Table 1.

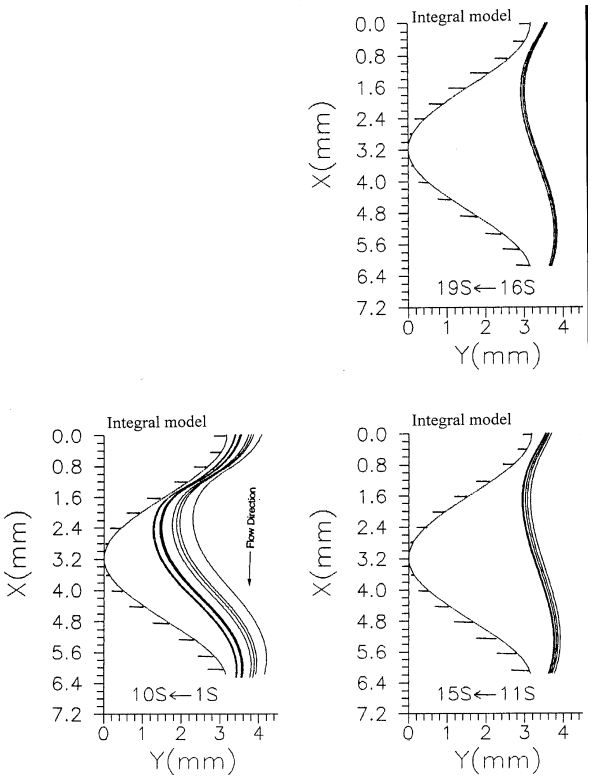

Fig. 3. Free surface profiles of the silicon oil film flowing over the corrugated surface with $A = 3.175$ mm and $L = 6.35$ mm. Calculations based on the integral model and flow rates corresponding to lines 1 S–19 S are given in Table 1.

in the calculation is given as $f(x) = 0.5[1-\cos(2\pi x)]$. We use the same values of physical properties as were listed by Zhao and Cerro (1992) (see Table 2).

It was difficult in the calculations to use exactly the same solid surface shape as in the experiments due to the large number of harmonics which were needed to approximate the corrugations. Taking into account this difference, it is possible to say that there is good agreement between all the corresponding plots in Figs. 2–4. The same conclusion follows from the comparison presented in Fig. 5. Line 1 and point 1 correspond to the dependence of the nondimensional film thickness maximum $\beta = (H_{\max}-H_{\min})/2H_0$ on Nusselt's thickness and line 2 and point 2 to that of the nondimensional film surface maximum $\beta = (h_{\max}-h_{\min})/2H_0$. Lines and points with lower index 'si' correspond to the calculations and experimental data for silicon oil, those with index 'g1A' for glycerol A and with index 'g1B' for glycerol B (see Table 2 for details).

In Fig. 6 the contour plots of the nondimensional streamline function are presented at three different Reynolds numbers. Calculations were carried out on the base of Navier–Stokes equations. Shape of the zero level contour line is identical to the solid wall surface and that of the unit level to the film free surface, as follows from (1). There are no stagnation zones for

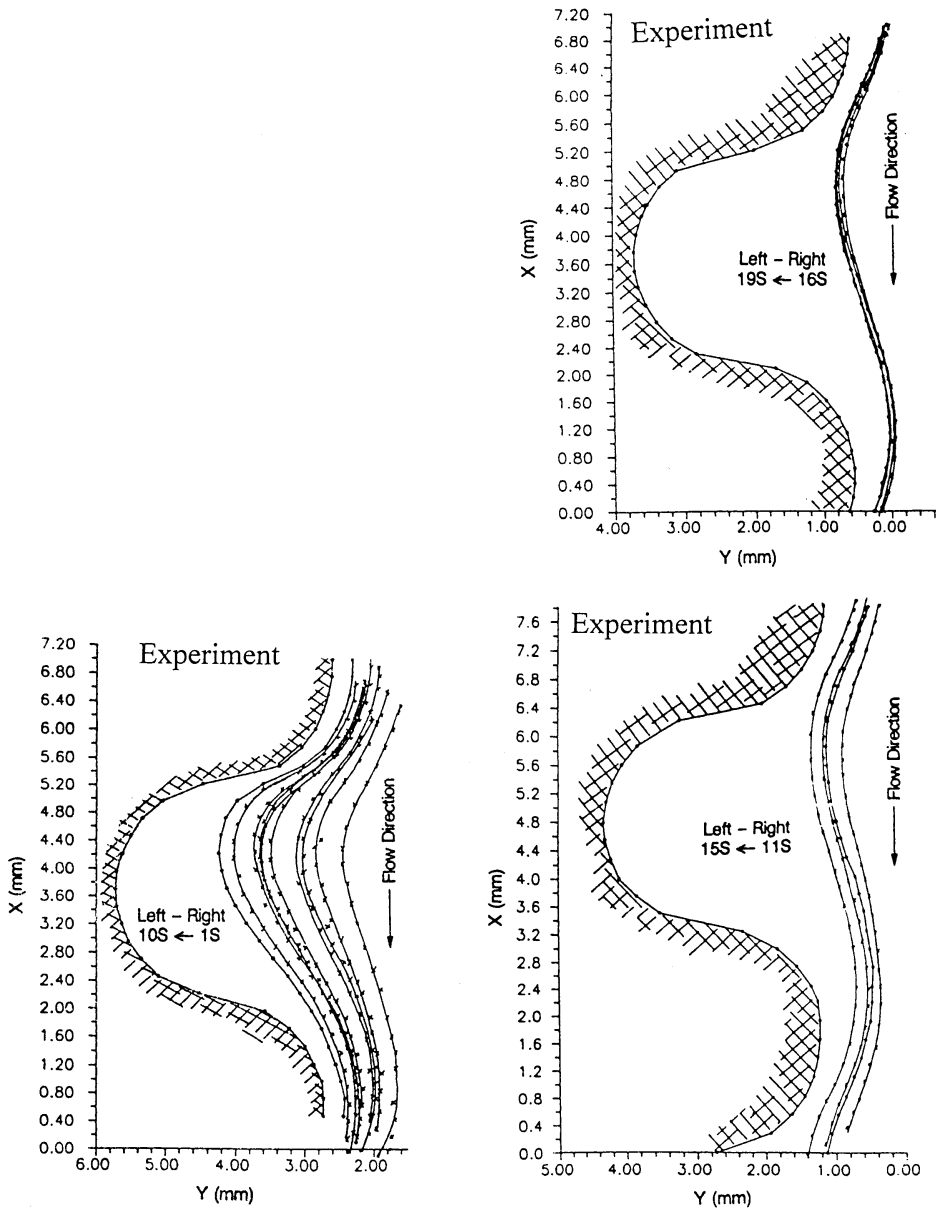

Fig. 4. Free surface profiles of the silicon oil film flowing over the corrugated surface with $A = 3.175$ mm and $L = 6.35$ mm. Experimental data obtained by Zhao and Cerro (1992). Flow rates corresponding to lines 1 S–19 S are given in Table 1.

this type of corrugation and for the liquid investigated. It is in agreement with Zhao and Cerro (1992) experiments.

In Fig. 7–12 the results of the hydrodynamics calculations of the film flowing down the corrugated surface with $A = 0.175$ mm, $L = 1.57$ mm and the same nondimensional shape $f(x) = 0.5[1-\cos(2\pi x)]$ are presented. In accordance with Zhao and Cerro (1992) this

Table 1
Reynolds numbers for the calculations and experiments presented in Figs. 2–4

No	Liquid	Reynolds number
1 S	Silicone oil	0.3870
2 S	Silicone oil	0.1657
3 S	Silicone oil	0.1284
4 S	Silicone oil	0.0890
5 S	Silicone oil	0.0265
6 S	Silicone oil	0.0221
7 S	Silicone oil	0.0199
8 S	Silicone oil	0.0193
9 S	Silicone oil	0.0060
10 S	Silicone oil	0.0043
11 S	Glycerol A	0.0139
12 S	Glycerol A	0.0093
13 S	Glycerol A	0.0069
14 S	Glycerol A	0.0047
15 S	Glycerol A	0.0038
16 S	Glycerol B	0.0019
17 S	Glycerol B	0.0015
18 S	Glycerol B	0.0011
19 S	Glycerol B	0.0010

corrugation is the *P*-surface. There is a special feature of the *P*-surface that the ratio of the corrugation amplitude to the period is small $A/L \ll 1$.

In Fig. 7, the contour lines of the streamline function are presented for the flow of a highly viscous liquid (silicon oil) over the *P*-surface. The shape of the film free surface is identical to the unit level contour line and one is very close to flat. There are no stagnation zones. Results of the calculations are in agreement with those of the experiments for this type of surface obtained by Zhao and Cerro (1992).

In Figs. 8 and 13–16, the results of investigation of the small viscosity and surface tension liquid film flow are presented. As an example, liquid nitrogen properties are used at the saturation line and at one atmosphere pressure (see Table 2 for details).

In Figs. 8 and 9 the comparison between the calculations based on the Navier–Stokes Eqs. (2)–(8) and integral model (11) are shown. Shapes of the free surface film at three

Table 2
Physical properties of the liquids used for the calculations and experiments in Figs. 2–5

Fluid	Silicone oil	Glycerin A	Glycerin B	Liquid nitrogen
Density (kg/m^3)	969	1261	1265	808
Viscosity (m^2/s)	$9.12\ 10^{-5}$	$3.6\ 10^{-4}$	$7.42\ 10^{-4}$	$1.82\ 10^{-7}$
Surface tension (N/m)	0.0214	0.0625	0.06	0.00887
Film number *Fi*	15.872	0.739	0.0359	$1.231\ 10^{11}$
Capillary const. $(\sigma/\rho g)^{1/2}$ (mm)	1.5	2.248	2.199	1.06
Viscous. const. $(3v^2/g)^{1/3}$ (mm)	1.365	3.41	5.522	0.0216

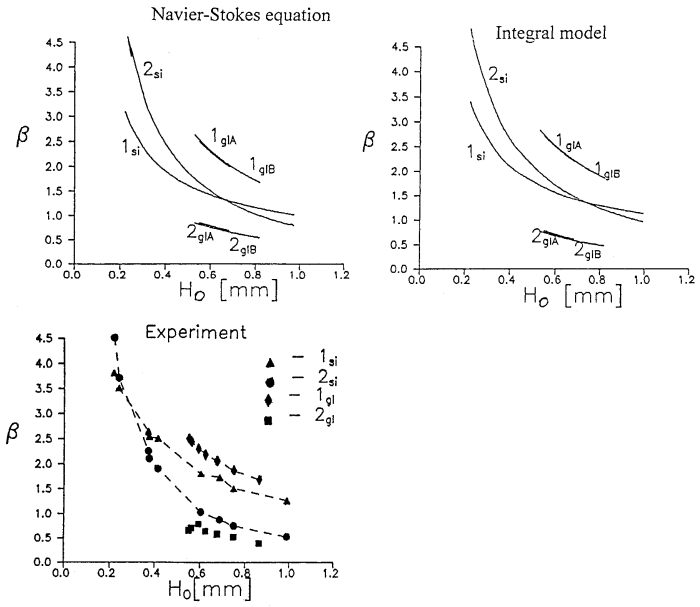

Fig. 5. Film flow of highly viscous liquid over the corrugated surface with $A = 3.175$ mm and $L = 6.35$ mm. Comparison of the calculations based on the Navier–Stokes and integral equations and Zhao and Cerro (1992) experiments.l Line 1 is $\beta = (H_{\max} - H_{\min})2H_0$, line 2 is $\beta = (h_{\max} - h_{\min})/2H_0$. Low index 'si' corresponds to the silicon oil, 'g1A' to glycerol A, 'g1B' to glycerol B (see Table 2).

different values of Reynolds number are presented in Fig. 8. Dependencies of the averaged nondimensional film thickness ($\langle H \rangle / H_0 = \int_0^1 H(x)\,\mathrm{d}x$) and those of the ratio $(h_{\max} - h_{\min})/A$ on Reynolds number are shown in Fig. 9.

There are several solutions of the integral model at $Re > 125$, for example; we have five different solutions at the same Reynolds number for $Re > 225$. For the integral model, the solutions from the range of large Reynolds numbers do not transform continuously into the solutions from the range of small Reynolds numbers with the parameter Re decreasing and we have two branches of solutions (see line 2 in Fig. 9).

Calculations based on the Navier–Stokes equations demonstrate that there is a single solution at one Reynolds number for all the range of Re investigated (see line 1 in Fig. 9).

Two qualitatively dissimilar areas in flow characteristic behavior can be distinguished within the studied range of Reynolds numbers. In the area of moderate Reynolds numbers, the flow is controlled significantly by the surface tension forces and there is good correspondence here between the Navier–Stokes solutions and the integral model (see profiles at $Re = 5$ in Fig. 8 and range $Re < 30$ in Fig. 9). With the Reynolds number increasing, the role of the inertia forces increases and they are dominant for the 'large' values of Re. There is essential disagreement between the Navier–Stokes and integral calculations in the range of 'large' Reynolds numbers in spite of the long-wave corrugation of the wall surface $A/L \ll 1$. Calculations according to the Navier–Stokes equations show that the free surface becomes flat with the Reynolds number increasing (see the film free surface profile at $Re = 400$ in the lower part of Fig. 8) which differs from the integral model calculations (profile at $Re = 400$ in the upper part of Fig. 8). The same conclusion follows from the results presented in Fig. 9. There

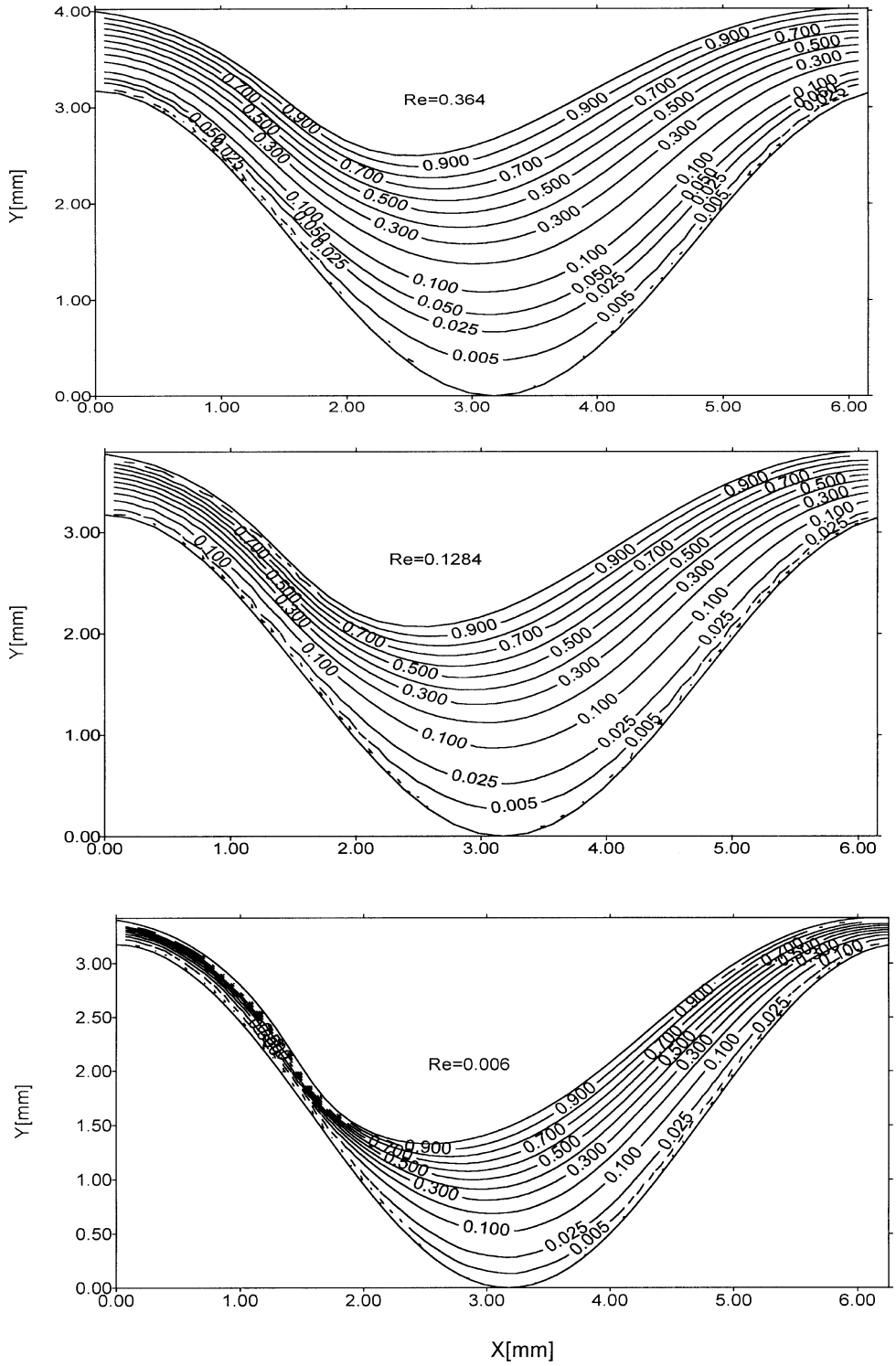

Fig. 6. Contour lines of streamline function. Film flow of silicon oil over the corrugated surface with $A = 3.175$ mm and $L = 6.35$ mm. Calculations based on the Bavier–Stokes equations.

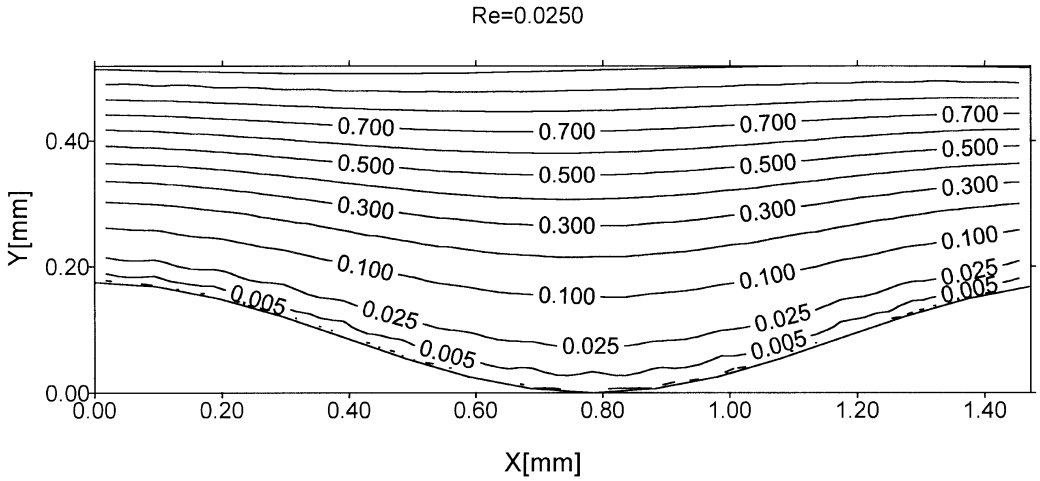

Fig. 7. Contour lines of streamline function. Film flow of silicon oil over the corrugated surface with $A = 0.175$ mm and $L = 1.57$ mm. Calculations based on the Navier–Stokes equations.

is the tendency, $(h_{\max} - h_{\min})/A \to 0$ with the Re increasing in this figure for the Navier–Stokes calculations and $(h_{\max} - h_{\min})/A \to \text{const}$, $\text{const} \neq 0$ for the integral model.

Averaged film thickness is always greater than the Nusselt thickness and their ratio increases rapidly with the Reynolds number decreasing in the range where the capillary forces are dominant. At small Reynolds numbers, areas of 'thick' film form in the surface cavities and areas of 'thin' film form on the tops.

Contour lines of streamline functions and their deformation with the Reynolds number increasing are presented in Fig. 10. The results are based on the Navier–Stokes equations and

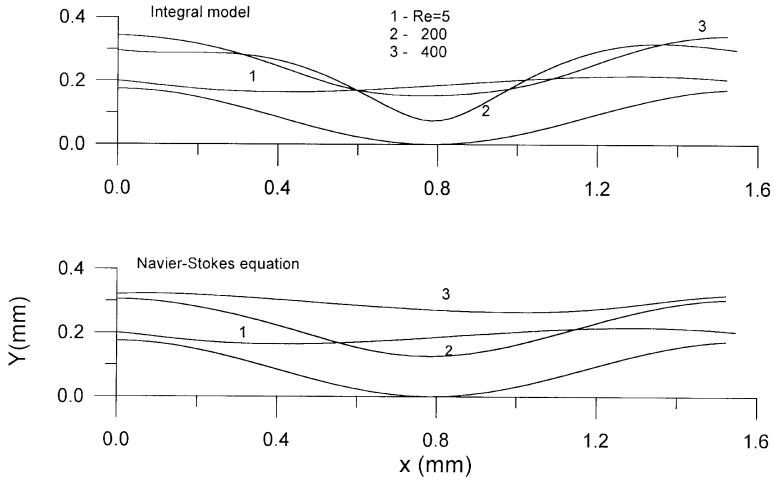

Fig. 8. Film flow of liquid with small viscosity over the corrugated sheet with $A = 0.175$ mm and $L = 1.57$ mm. Profiles of the free surface at various Reynolds numbers calculated according to the Navier–Stokes and integral equations.

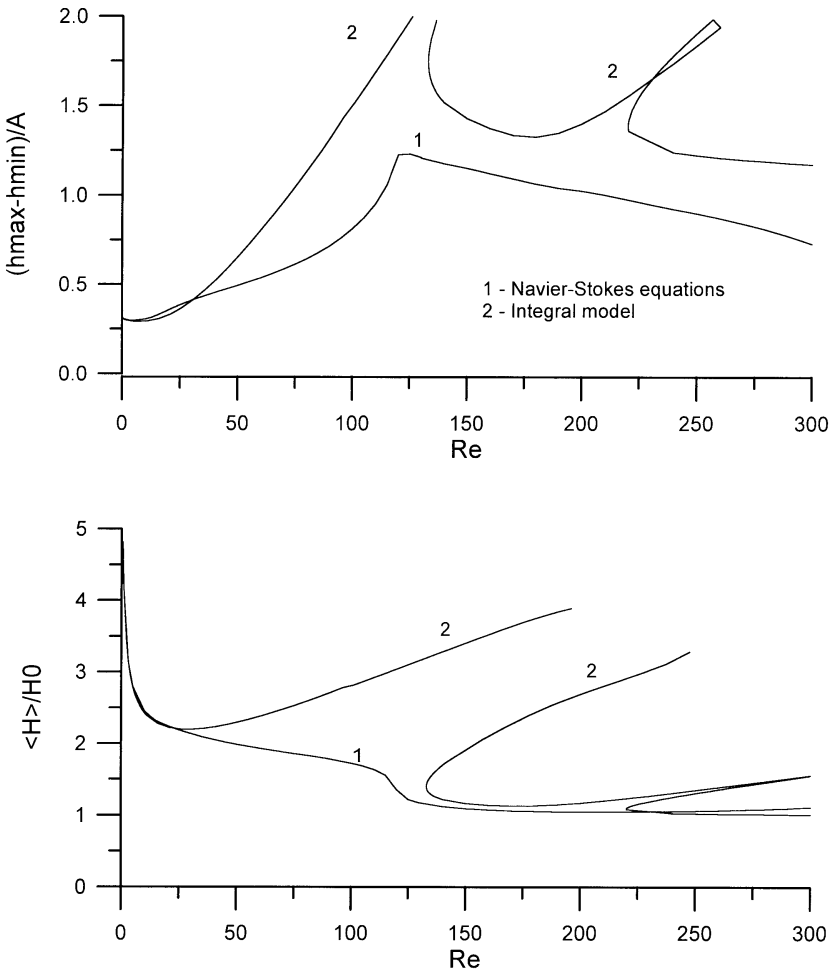

Fig. 9. Film flow of liquid with small viscosity over the corrugated sheet with $A = 0.175$ mm and $L = 1.57$ mm.

allow us to explain why the integral approach gives wrong conclusion for the 'large' value of Re ($Re > 30$). The main effect, which is not taken into account by the integral approach, is the presence of the stagnation zones where the liquid circulates without flowing from one cavity to another (the stagnation or recirculating zone is bounded by zero contour lines in Fig. 10).

There are at least two ranges of the Reynolds number where we have no stagnation zones as follows from the results in Fig. 10. Figs. 11 and 12 show the range of Re where the stagnation zone disappears with the smaller step of the Reynolds number. It is followed from Figs. 10–12 that the stagnation zone is born on the negative slope ($df/dx < 0$) of the corrugations and disappears on the positive side of the corrugation ($df/dx > 0$).

It is interesting to note that, for the Reynolds number close to the value we obtained where the stagnation zone disappears, the resonance phenomenon between a wavy wall and the free surface was recently predicted by Bontozoglou and Papapolymerou (1997).

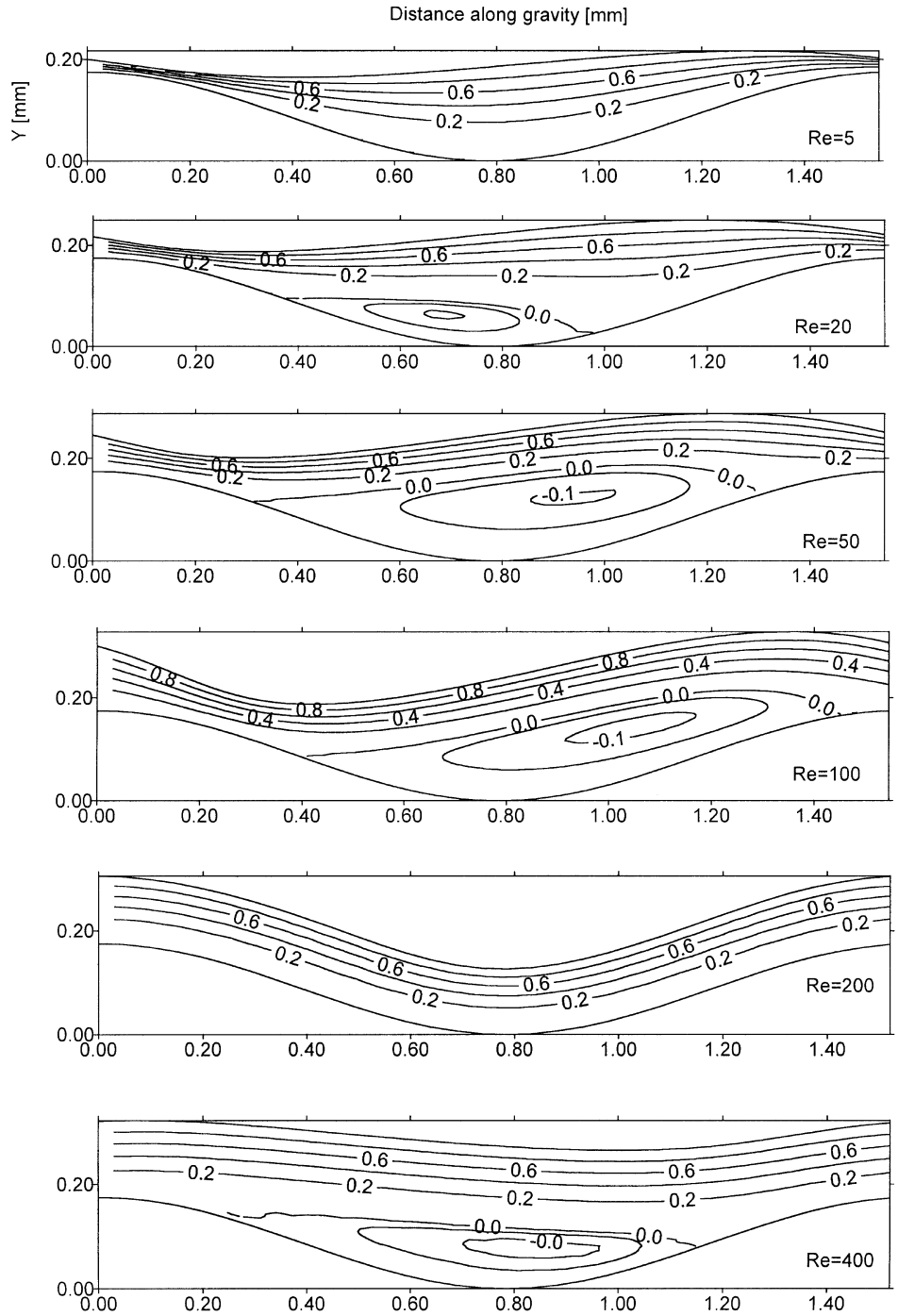

Fig. 10. Contour lines of streamline function. Film flow of liquid with small viscosity over the corrugated surface with $A = 0.175$ mm and $L = 1.57$ mm. Calculations based on the Navier–Stokes equations.

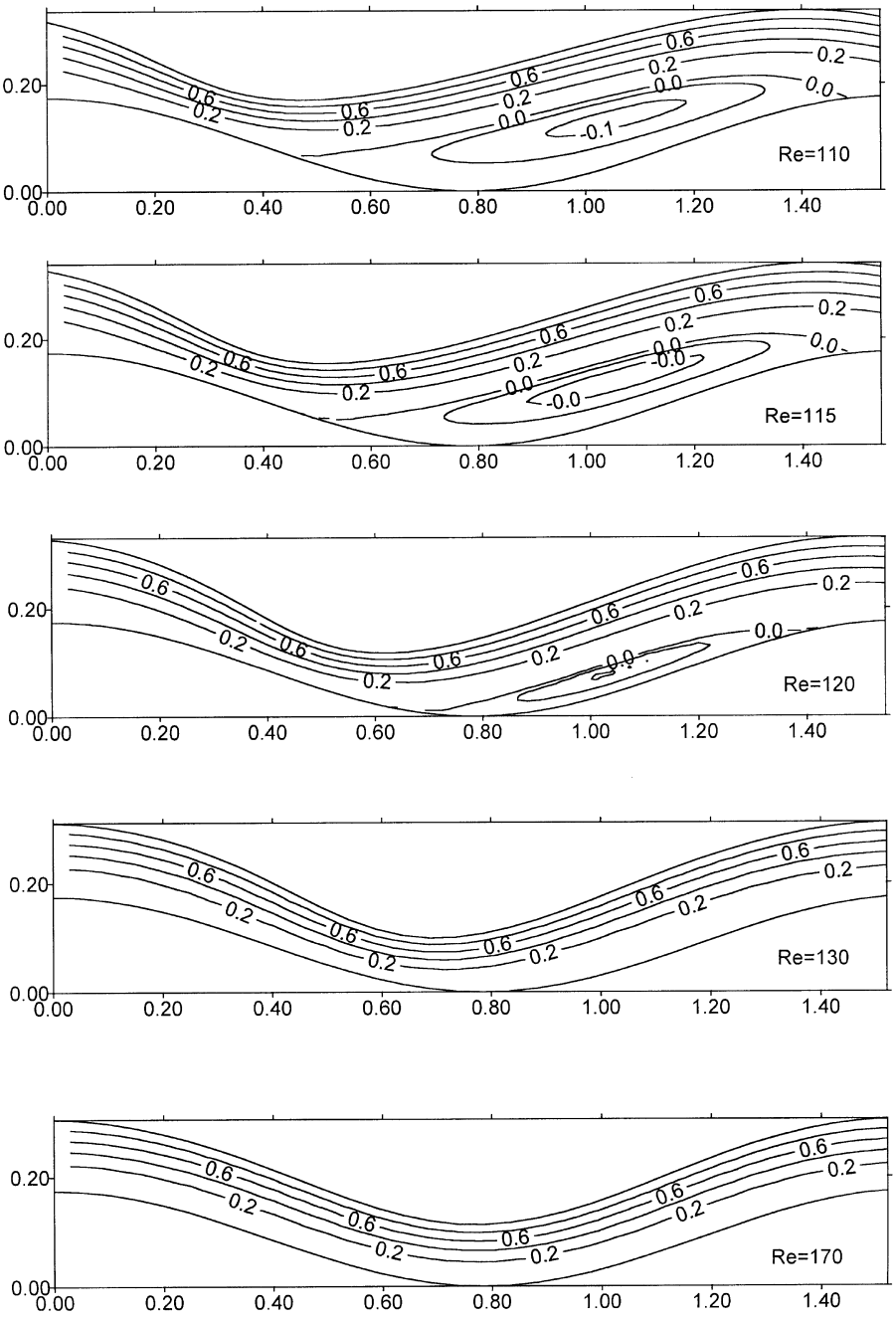

Fig. 11. Contour lines of streamline function. Film flow of liquid with small viscosity over the corrugated surface with $A = 0.175$ mm and $L = 1.57$ mm. Calculations based on the Navier–Stokes equations.

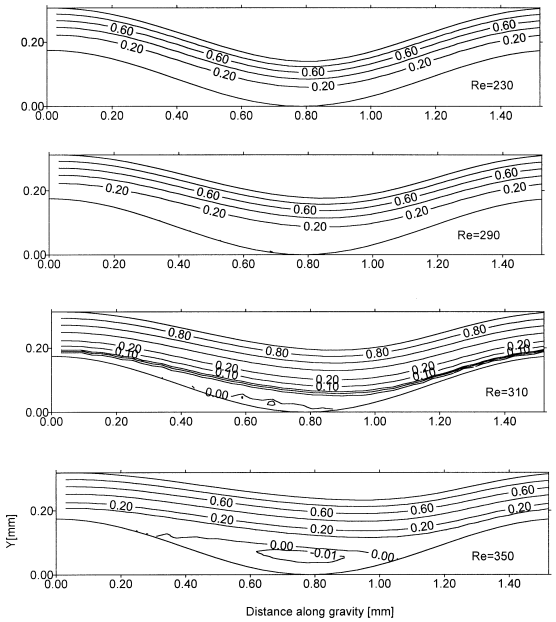

Fig. 12. Contour lines of streamline function. Film flow of liquid with small viscosity over the corrugated surface with $A = 0.175$ mm and $L = 1.57$ mm. Calculations based on the Navier–Stokes equations.

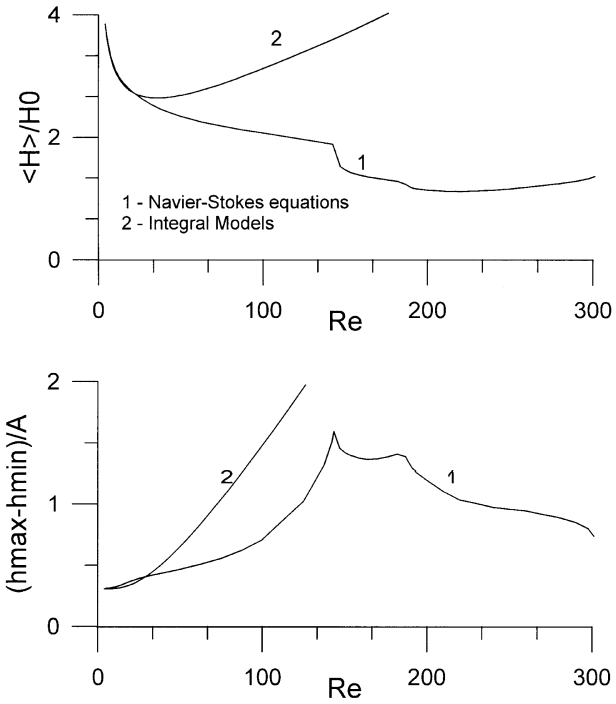

Fig. 13. Film flow of liquid with small viscosity over the surface with a more complex shape of corrugations than the sinusoidal profile. Amplitude and period of corrugations are $A = 0.175$ mm, $L = 1.57$ mm.

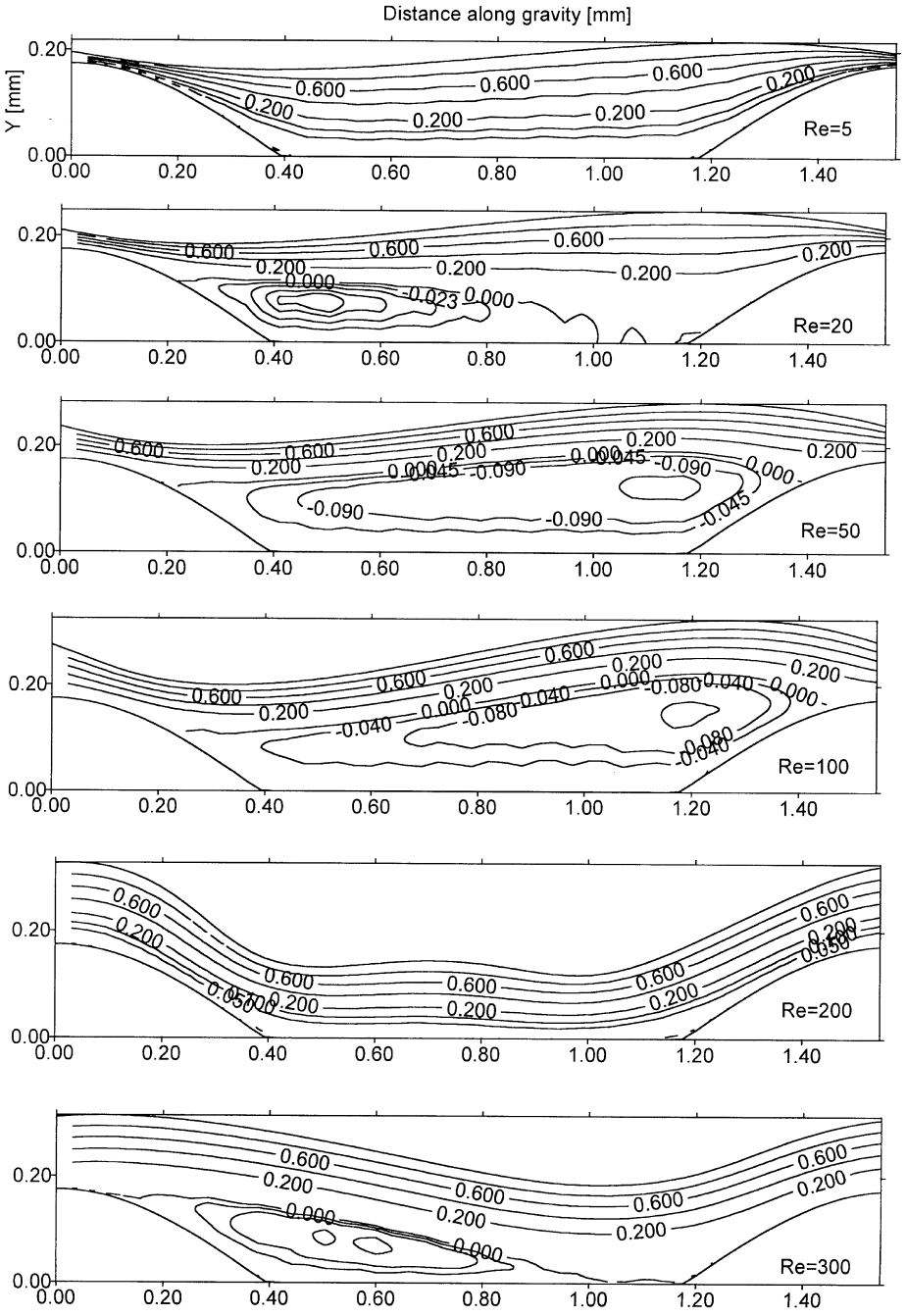

Fig. 14. Contour lines of streamline function. Film flow of liquid with small viscosity over the surface with a more complex shape of corrugations than the sinusoidal profile. Amplitude and period of corrugations are $A = 0.175$ mm, $L = 1.57$ mm. Calculations based on the Navier–Stokes equations.

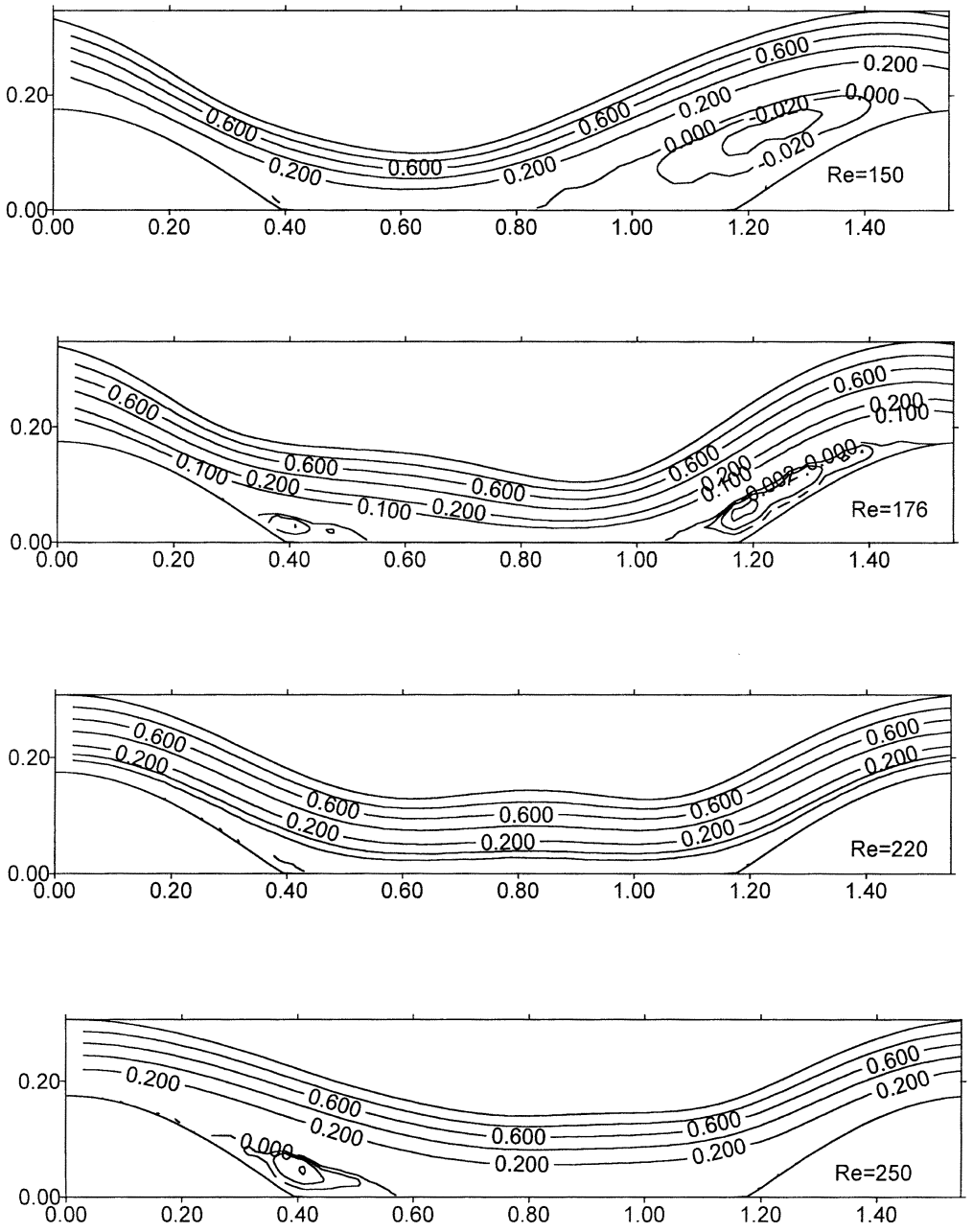

Fig. 15. Contour lines of streamline function. Film flow of liquid with small viscosity over the surface with a more complex shape of corrugations than the sinusoidal profile. Amplitude and period of corrugations are $A = 0.175$ mm, $L = 1.57$ mm. Calculations based on the Navier–Stokes equations.

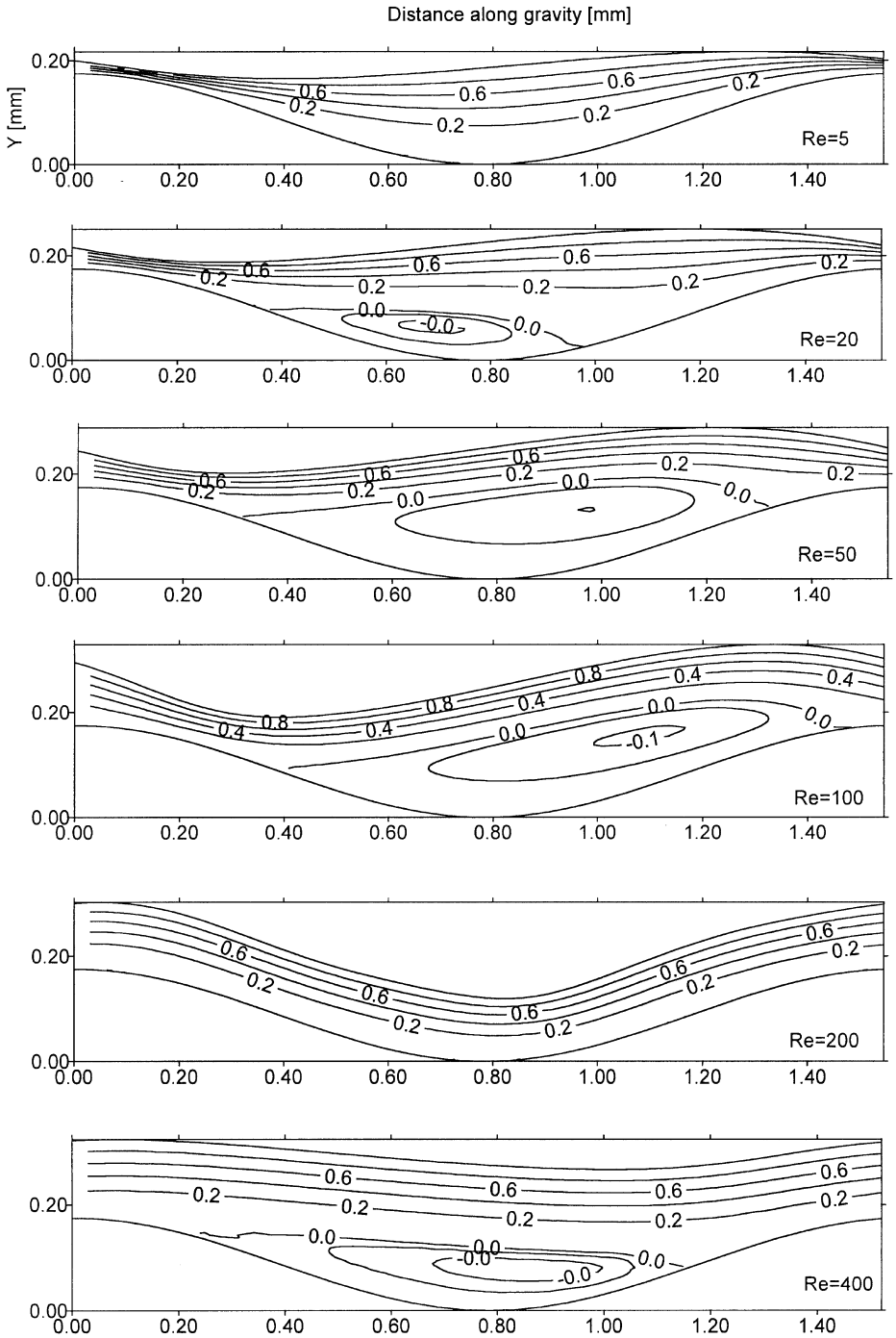

Fig. 16. Contour lines of streamline function. Film flow of liquid with small viscosity over the corrugated surface with $A = 0.175$ mm and $L = 1.57$ mm. Calculations based on the simplified Navier–Stokes equations.

Results of the investigation of the wall corrugation shape influence on film flow hydrodynamics and on comparison between the integral approach and Navier–Stokes equations are given in Figs. 13–15. The dimensionless shape of the corrugations is a 'cut' sinusoidal profile and harmonics of the Fourier expansion are as follows:

$$f_0 = \frac{1}{\pi}; \quad Re(f_n) = \frac{1}{4}\left\{ s\left(\frac{n-1}{2}\right) + s\left(\frac{n+1}{2}\right)\right\}; \quad Im(f_n) = 0; \quad n = 1, \ldots, \frac{N}{2} - 1;$$

$$s(x) = \frac{\sin \pi x}{\pi x}.$$

Amplitude and period of the corrugations are 0.175 mm and 1.57 mm, respectively. Results presented in Figs. 13–15 are qualitatively the same as have been discussed for the flow over a sinusoidal profile. Let us emphasize that there are also two ranges of Reynolds number where we have no stagnation zones.

5. Simplified system of the governing equations

One of the most interesting results of the paper is that, starting from some value of Reynolds number, the essential disagreement between the predictions of the integral model and Navier–Stokes equations is obtained in spite of the small ratio $A/L \ll 1$. There is the important question of how to correctly use the small value of the parameter A/L and to simplify Navier–Stokes equations without loss of the stagnation zone prediction. To investigate this problem, we successively reduce the system of Eqs. (2)–(8) discarding terms $O(\varepsilon)$ and comparing the results of the calculations with those of the Navier–Stokes equations over a wide range of Reynolds numbers. As a result, it is demonstrated that the simplest system of equations is as follows:

$$u\frac{\partial u}{\partial x} + v\frac{\partial u}{\partial y} = -\frac{1}{\rho}\frac{\partial P}{\partial x} + g + \nu\frac{\partial^2 u}{\partial y^2}; \quad u\frac{\partial v}{\partial x} + v\frac{\partial v}{\partial y} = -\frac{1}{\rho}\frac{\partial P}{\partial y}; \quad \frac{\partial u}{\partial x} + \frac{\partial v}{\partial y} = 0;$$

$$u = v = 0, \quad y = f(x);$$

$$P = P^{(V)} - \sigma\frac{\mathrm{d}^2 h}{\mathrm{d}x^2}, \quad \frac{\partial u}{\partial y} = 0, \quad v = u\frac{\mathrm{d}h}{\mathrm{d}x}, \quad y = h(x);$$

and in nondimensional form

$$\frac{\partial u}{\partial x} + \eta_x\frac{\partial u}{\partial \eta} + \eta_y\frac{\partial v}{\partial \eta} = 0; \tag{12}$$

$$\varepsilon^2\left[H\frac{\partial uv}{\partial x} + H\eta_x\frac{\partial uv}{\partial \eta} + \frac{\partial v^2}{\partial \eta}\right] = -\frac{\partial P}{\partial \eta}; \tag{13}$$

$$\frac{\partial u^2}{\partial x}+\eta_x\frac{\partial u^2}{\partial \eta}+\eta_y\frac{\partial vu}{\partial \eta}=-\frac{\partial P}{\partial x}-\eta_x\frac{\partial P}{\partial \eta}+\frac{1}{\varepsilon Re}\left[3+\eta_y^2\frac{\partial^2 u}{\partial \eta^2}\right]; \tag{14}$$

$$u(x,\eta)=v(x,\eta)=0, \quad \text{for } \eta=0; \tag{15}$$

$$P-P^{(V)}=-\varepsilon^2 We\left[\frac{\mathrm{d}^2 H}{\mathrm{d}x^2}+\frac{1}{\varepsilon_1}\frac{\mathrm{d}^2 f}{\mathrm{d}x^2}\right], \quad \frac{\partial u}{\partial \eta}=0, \quad \text{for } \eta=1. \tag{16}$$

In Fig. 16, the contour lines of the streamline functions and their transformation with the Reynolds number increasing are shown. Calculations are based on the reduced system of (12)–(16) and the comparison with the results presented in Fig. 10 demonstrates good agreement.

Further simplification of (12)–(16) leads to the loss of the stagnation zone description and gives us the essential disagreement with the calculations based on the Navier–Stokes equations.

6. Conclusion

Theoretical analysis of a viscous liquid film flowing down a vertical one-dimensional periodic surface is carried out. The investigation is based on both Navier–Stokes and integral equations and is performed over a wide range of Reynolds number and surface geometry characteristics, taking into account viscosity, inertia and surface tension. Results presented in the paper allow the following conclusions to be drawn:

1. Two qualitatively dissimilar areas in flow characteristic behavior can be distinguished within the studied range of Reynolds numbers. In the area of moderate Reynolds numbers, the flow is controlled significantly by the forces of surface tension, and in the area of large *Re* by inertia forces.
2. The comparison between the results obtained on the basis of the integral model and Navier–Stokes equations demonstrates that the integral approach is correct in the area where the flow is defined mainly by surface tension forces.
3. The calculations show that, while increasing the Reynolds number, the free surface 'straightens' and becomes parallel to the x-axis. At small Reynolds numbers, areas of 'thick' film form in the surface cavities and areas of 'thin' film form on the tops. Average film thickness is always greater than Nusselt thickness and, as *Re* decreases, this difference increases due to the presence of 'thick' film in the cavities.
4. For the flow of liquid with small viscosity, two ranges of *Re* are found where the stagnation zones exist. Flow of the highly viscous liquid over the same corrugations is without the recirculation zones.

References

Alekseenko, S.V., Nakoryakov, V.E., Pokusaev, B.G., 1992. Wavy Liquid Film Flow, 255. Nauka, Novosibirsk.
Bontozoglou, V., Papapolymerou, G., 1997. Laminar film flow down a wavy incline. Int. J. Multiphase Flow 1, 69–79.
Fulford, G.D., 1964. The flow of liquids in thin films. Adv. Chem. Eng. 5, 151–236.
Kang, F., Chen, K., 1995. Gravity-driven two-layer flow down a slightly wavy periodic incline at low Reynolds numbers. Int. J. Multiphase Flow 3, 501–513.
Nusselt, W., 1916. Die Oberflachenkondensation des Wasserdampfles. Teil I, II.Z.VDI 27 (541), 28, 569–576.
Pozrikidis, C., 1988. The flow of a liquid film along a periodic wall. J. Fluid Mech. 188, 275–300.
Shetty, S., Cerro, R.L., 1993. Flow of a thin film over a periodic surface. Int. J. Multiphase Flow 6, 1013–1027.
Trifonov Ya, Yu, Tsvelodub Yu, O., 1991. Non-linear waves on the surface of a falling liquid film, Part 1. Waves of the first family and their stability. J. Fluid Mech. 229, 531–554.
Wang, C.Y., 1981. Liquid film flowing slowly down a wavy incline. AIChE J. 27, 207–212.
Zhao, L., Cerro, R.L., 1992. Experimental characterization of viscous film flows over complex surfaces. Int. J. Multiphase Flow 6, 495–516.